Properties of the humic-like material arising from the photo-transformation of L-tyrosine

(Article begins on next page)

19 September 2024

Properties of the humic-like material arising from the photo-transformation of L-tyrosine.

Silvia Berto[1*], Elisa De Laurentiis[1], Tiziana Tota[1], Enrico Chiavazza[1], Pier Giuseppe Daniele[1], Marco Minella[1], Marco Isaia[2], Marcello Brigante,[3] Davide Vione[1*]

[1]*Università di Torino, Dipartimento Chimica, via P. Giuria, 7 – 10125 Torino, Italy.*
[2]*Università di Torino, Dipartimento di Scienze della Vita e Biologia dei Sistemi, Via Accademia Albertina 13, Torino 10123, Italy.*
[3]*Clermont Université, Université Blaise Pascal, Institut de Chimie de Clermont-Ferrand, BP 10448, F-63000 Clermont-Ferrand, France; and CNRS, UMR 6296, ICCF, BP 80026, F-63177 Aubière, France.*

* Address correspondence to either author. *silvia.berto@unito.it*; *davide.vione@unito.it*

Abstract

The UVB photolysis of L-tyrosine yields species with fluorescence and absorption spectra that are very similar to those of humic substances. By potentiometric measurements, chemical modelling and the application of NMR, mass spectrometry and laser flash photolysis, it was possible to get insights into the structural and chemical properties of the compounds derived by the L-tyrosine phototransformation. The photolytic process follows aromatic-ring hydroxylation and dimerization. The latter is presumably linked with the photoinduced generation of tyrosyl (phenoxy-type) radicals, which have a marked tendency to dimerize and possibly oligomerize. Interestingly, photoinduced transformation gives compounds with protogenic and complexation capabilities similar to those of the humic substances that occur naturally in surface waters. This finding substantiates a new and potentially important abiotic (photolytic) pathway for the formation of humic compounds in surface-water environments.

Keywords

Photochemistry; Protogenic sites; Ligands for metals; Aromatic aminoacids; Surface waters.

1. Introduction

Humic substances (HS) are important components of the chromophoric dissolved organic matter (CDOM) that occurs in surface waters (Ma et al., 2010; Xiao et al., 2013). HS play key roles in surface-water ecosystems because, as major sunlight absorbers, they can limit the penetration of harmful UVB radiation into the water column (Sommaruga and Augustin, 2006; Piccini et al., 2009; Uusikivi et al., 2010). Moreover, HS may act as solvents for water-insoluble organic pollutants and as ligands for metals and even inorganic nanoparticles. In all these cases, HS can allow the aqueous-phase transport of otherwise insoluble harmful species (Senesi, 1992; Westerhoff and Nowack, 2013; Prado et al., 2014). An additional issue is that the absorption of sunlight by HS causes the production of photoactive transients: the hydroxyl radical, $^{\bullet}OH$; singlet oxygen, $^{1}O_2$; CDOM triplet states, $^{3}CDOM^*$ and, in the presence of inorganic carbon, the carbonate radical, $CO_3^{-\bullet}$. These transients are involved into the indirect photodegradation of many priority and emerging pollutants, but they can also induce the formation of harmful by-products (Latch and McNeill, 2006; Cavani et al., 2009; Minella et al., 2013; Cawley et al., 2015).

HS are usually thought to originate from the microbial decomposition of organic material that occurs in soil (allochthonous HS, which reach water bodies by *e.g.* runoff) and surface waters (autochthonous HS) (Xu and Zheng, 2003; Su et al., 2015). However, recent research suggests that compounds with fluorescence properties that are very similar to those of humic and fulvic acids can be formed by photolysis (or photoinduced oxidation) of phenolic compounds and of amino acids such as tyrosine and tryptophan (De Laurentiis et al., 2013a/b/c; Bianco et al., 2014). In the latter case, the amino acids have been irradiated by UVB light and their direct photolysis has induced the formation of compounds with fluorescence emission in the HS region, as suggested by their excitation-emission matrix (EEM) fluorescence spectra. Moreover, the irradiated material was able to photoproduce reactive transient species ($^{1}O_2$, $^{3}CDOM^*$), which was not the case for the original amino acids (Bianco et al., 2014). Despite these analogies, the extent to which the photogenerated

compounds can be assimilated to HS and, therefore, the significance of the possible abiotic pathway leading to HS production have been scarcely clarified. Indeed, it is essential to assess whether the photogenerated material may have further properties in common with HS.

The definition of HS is currently an operational one, *(i)* because they are not compounds of definite chemical structure (which can vary depending on the environment), and *(ii)* because their structure is still insufficiently elucidated despite recent important advances in the so-called humeomics science (Piccolo, 2001; Nebbioso and Piccolo, 2011; Nebbioso et al., 2014). Nevertheless, some chemical properties such as the presence of carboxylic and phenolic groups, the acid-base behaviour and the ability to form complexes with metal cations are distinctive features of HS. While previous work reveals that compounds sharing some HS-like properties can be formed upon irradiation of amino acids, some important chemical properties that could substantiate their assimilation to HS have not been elucidated so far: they include the occurrence of relevant functional groups, the protogenic properties and the metal complexation capabilities.

Therefore, the present paper is aimed at better characterizing the compounds formed upon irradiation of the amino-acid L-tyrosine. Amino acids may be present in surface waters as components of proteins and peptides at concentrations ranging within 20-6000 μg L^{-1} (Thurman, 1985) or in the free form, in which case they can account for about 6% of the DON (Dissolved Organic Nitrogen) (Bronk, 2002). Previous works studied the indirect photodegradation of amino acids, or dipeptides, evaluating the effect of pH (Saprygina et al., 2014), Reactive Oxygen Species (ROS) and Dissolved Organic Matter (DOM) (Boreen, et al., 2008; Plowman et al., 2013; Posadaz et al., 2004) on the photooxidation kinetics. Besides, it is known that the tyrosine is one of the photosensitive amino acids and it is subjected to direct photodegradation under solar-simulated conditions (Boreen, et al., 2008). However, information on the nature of the tyrosine photooxidation products is still lacking. Early work has suggested that the phototransformation of tyrosine might proceed in a similar way as the biosynthesis of melanin, through the intermediate formation of 3,4-dihydroxyphenylalanine (DOPA) (Bosetto et al., 1997). However, recent research has shown that a

possible DOPA pathway cannot account for the formation of substances with humic fluorescence (Bianco et al., 2014). In any case, the phototransformation of amino acids has an environmental interest in addition to the mechanistic one, because of its important but variable consequences on the bacterial communities (Amado et al., 2015), also concerning the chemistry and the photochemistry of surface waters. For the reported reasons, additional investigations on this topic should provide insight into the environmental significance of possible abiotic (photochemical) processes of HS formation. Moreover, amino acids, and tyrosine in particular, are involved in Cu(II) complexation (He et al., 2014), and also the binding of Cu(II) to HS is thought to occur through nitrogenous ligands similar to those of amino acids (Croue et al., 2003).

This works aims at providing additional insight into the photochemical formation of humic-like substances from tyrosine, with particular emphasis on the reaction pathways (how is tyrosine phototransformed) and on the humic nature of the photogenerated material. In the latter case, the ability of the irradiated solutions to undergo acid-base chemistry and to complex metal ions (Cu) will be assessed, as these are important features of natural humic substances.

2. Experimental Section

2.1. Chemicals

Tetraethyl ammonium chloride (TEACl, ≥98.5%), copper chloride (99%), potassium carbonate (>99%), sodium acetate (>98%), disodium hydrogen phosphate (>99%), formic acid (~98%), trifluoroacetic acid (99%), methanesulfonic acid (>99.5%), perchloric acid (70%) and methanol (>99.8%) were from Sigma Aldrich (St. Louis, Missouri, US). Phosphoric acid (85%) and acetic acid (100%) were provided by Carlo Erba Reagents (Cornaredo, Italy). L-tyrosine (>99%) was from Merck (Darmstadt, Germany). Deuterated dimethyl sulfoxide, DMSO-d_6, was from Eurisotop, France. Standard KOH and HCl solutions were prepared by diluting Merck or Sigma Aldrich concentrated products, and they were standardized against potassium hydrogen phthalate (Sigma

Aldrich, ≥99.5%) and sodium carbonate (Sigma Aldrich, ≥99.5%), respectively. Grade-A glassware and ultra-pure water (Milli-Q, Millipore) were used for all the solutions.

2.2. Irradiation experiments

To evaluate the transformation kinetics, a solution (80 mL) of L-tyrosine 1.0 mmol L^{-1} was placed into a square Pyrex glass bottle (capacity 100 mL) and irradiated under a solar simulator (Solarbox, CO.FO.ME.GRA., Milan, Italy) equipped with a 1500 W Philips xenon lamp and a 320 nm cut-off filter. This filter transmits 50% of radiation at 320 nm, its transmittance being lower (and reaching up to zero) below 320 nm and higher above it. The concentration and the volume of the irradiated solutions were chosen in order to allow the successive potentiometric investigation. Each bottle was placed so as to lie down horizontally on one of its flat sides, and irradiation occurred through the opposite side that acted as optical window. Lamp radiation was vertically incident over the solutions and the optical path length was 1.95 cm. The UV irradiance reaching the bottles was 28.0 ± 1.6 W m^{-2}, measured with a CO.FO.ME.GRA. (Milan, Italy) multimeter equipped with a UV probe that is sensitive to radiation in the 295-400 nm interval. The photon flux in solution was actinometrically determined with the ferrioxalate method (Kuhn et al. 2004), taking into account the wavelength-dependent quantum yield of Fe^{2+} photogeneration and the overlap between ferrioxalate absorption and lamp emission (Albinet et al. 2010). The lamp photon flux density incident on the irradiated solutions ($p°(\lambda)$), determined by combining actinometry results with spectral measurements using an Ocean Optics USB2000 CCD spectrophotometer, is reported in Figure 1a. The photon flux emitted by the lamp below 400 nm ($\int_{300nm}^{400nm} p°(\lambda)\,d\lambda$) is 2.2·10^5 Einstein L^{-1} s^{-1}.

The L-tyrosine solutions were irradiated in the Solarbox for a variable amount of time (0 − 72 h, corresponding to a fluence of up to 7.3·10^6 J m^{-2}). The maximum adopted fluence in the irradiation experiments corresponds to about a week of surface-water illumination under fair-weather conditions, in mid-July at mid latitude (Bodrato and Vione, 2014).

The solutions were magnetically stirred during irradiation, and no pH control was carried out unless otherwise reported. pH-buffers were not used to control the pH during the irradiation in order to avoid their interference in the successive titrations. However, we verified that there were no changes in the fluorescence spectra between the solutions at natural (pH 5.9 or 3.9 for not treated tyrosine and irradiated tyrosine solutions, respectively) and neutral pH. Dark runs were carried out by wrapping the bottles with aluminium foil and by placing them under the lamp with magnetic stirring.

The irradiated solutions were directly analyzed, as reported below, or transferred to a round-bottomed flask and lyophilized (using a EC-Modulyo device, EC Apparatus, NY, USA). The brown powders thus obtained were fractionated for NMR and mass spectrometric characterization.

2.3. Analytical determinations

After the scheduled irradiation times, L-tyrosine was quantified by high-performance liquid chromatography with diode array detection (HPLC-DAD). The VWR-Hitachi Elite LaChrom instrument was equipped with L-2130 quaternary pump for low-pressure gradients (with Duratec external degassing unit), L-2200 autosampler, L-2300 column oven (kept at 40 °C) and L-2455 DAD detector. The column used was a Merck LiChroCART RP-18 (125 mm × 4 mm × 5 µm), with 60 µL injection volume and a flow rate of 1.0 mL min^{-1}. All samples were eluted with isocratic mixtures of methanol and 5 mM acetate buffer (pH 4) with a ratio of 2 : 98, and detected at 274 nm (retention time 2.6 min).

The Total Inorganic Nitrogen (NO_2^-, NO_3^-, NH_4^+) was determined by ion chromatography with electrochemical suppression. The adopted apparatus was a Dionex DX500 chromatograph, equipped with a GP40 gradient pump, ED40 electrochemical detector and an injector with a 100 µL loop. For the measurement of nitrate and nitrite it was adopted an Ion Pac AG9-HC-AS9-HC guard column + column with 9 mmol L^{-1} K_2CO_3 as eluent at 1.0 mL min^{-1} flow rate, and a conductivity suppression unit ASRS 300. The analysis of ammonium was performed with Ion Pac CG12A-

CS12A guard column + column, 20 mmol L^{-1} methanesulfonic acid as eluent at a 1.0 mL min^{-1} flow rate, and a conductivity suppression unit CERS 500.

A mass profile of the irradiated solutions was obtained with a Thermo Finnigan Advantage Max Ion trap spectrometer, equipped with an ESI ion source used in positive ion acquiring mode. Nitrogen was used as sheath and auxiliary gas. Sheath gas flow rate was set at 25 (arbitrary unit), auxiliary gas flow rate at 5 (arbitrary unit). The tuning parameters were: capillary voltage at 25 V, tube lens offset at 5.00 V. The source voltage was set to 4.5 KV and the capillary temperature was maintained at 250 °C. The lyophilized product (see section *2.2 Irradiation experiments*) was dissolved in 50/50 water/methanol – formic acid 0.1%, then it was injected into the mass analyzer.

2.4. Spectroscopic characterization of the irradiated systems

The absorption spectra (230 – 600 nm) were recorded with a Jasco V-550 UV-vis double-beam spectrophotometer, adopting Hellma quartz cuvettes with 1.000 cm optical path length. A full baseline was taken before each absorbance measurement, to compensate for the asymmetry of photomultipliers, using two cuvettes filled with Milli-Q water. Each absorbance spectrum was then taken against the reference cuvette filled with Milli-Q water.

A Varian Cary Eclipse fluorescence spectrofluorimeter was also used, adopting a 5 nm bandpass on both excitation and emission. The bandpass choice was motivated by the high fluorescence intensity of the samples. The fluorescence Excitation-Emission Matrix (EEM) was obtained at 5 nm intervals for excitation wavelengths from 200 to 500 nm and emission ones from 220 to 600 nm. When required, the pH of the solutions was controlled with phosphate buffer at pH 7.

Identification of fluorescent constituents in the water samples was performed on the basis of literature data (Coble, 1996), using the main fluorescence contours to identify the relevant peaks. Before and after each EEM measurement, the intensity of the Raman signal of water was used to check the stability of the instrumental conditions.

Nephelometric measures were carried out with a DRT 1000 nephelometer by HF Instrument, calibrated in standard formazine units (NTU) as prescribed by the 7025 ISO norm (ISO, 1999). Particle diameters were determined by Dynamic Laser Light Scattering using an ALV–NIBS instrument, measuring scattered light for at least 20 s at 298 K.

In order to collect the NMR spectra of the degradation products, the lyophilized material was dissolved in 580 μL of DMSO-d_6, added with 20 μL of trifluoroacetic acid (TFA) and vortexed for 30" (vortex VWR VV3) or until the suspension was completely dissolved. The sample was then transferred into a common NMR glass tube and the spectra were recorded on a Bruker AVANCE200 spectrometer (4.7 T), thermostated at 298 K.

2.5. *Laser flash photolysis experiments*

Laser flash photolysis (LFP) experiments were performed at 266 nm excitation using the fourth harmonic of a Quanta Ray GCR 130-01 Nd:YAG laser system instrument, used in a right-angle geometry with respect to the monitoring light beam. The Nd:YAG laser emits radiation at 1064 nm, and by use of suitable non-linear optical materials the radiation frequency can be doubled (532 nm), tripled (355 nm) or quadrupled (266 nm). Tyrosine is unfortunately unable to absorb radiation of 355 nm, thus the fourth harmonic at 266 nm had to be used. While belonging to the UVC range, the 266 nm radiation excites the same absorption band that is also responsible of tyrosine absorption in the UVB region (see Figure 1b). Therefore, one does not expect important differences in tyrosine photochemistry at 266 nm or in the UVB (Turro et al., 1978). The single pulses were *ca*. 9 ns in duration, with energy of ~60 mJ pulse^{-1}. To limit degradation during transient acquisition due to the multiple laser shots, it was used a flow cell connected to a peristaltic pump to have a fresh solution every two-three measurements. The transient absorbance at the pre-selected wavelength was monitored by a detection system consisting of a pulsed xenon lamp (150 W), monochromator and a photomultiplier (1P28). A spectrometer control unit was used for synchronizing the pulsed light source and programmable shutters with the laser output. The signal from the photomultiplier was

digitized by a programmable digital oscilloscope (HP54522A). A 32 bits RISC-processor kinetic spectrometer workstation was used to analyse the digitized signal.

Tyrosine spectra were acquired each 10 nm in the wavelength range 300-600 nm. All the experiments were performed at ambient temperature (295 ± 2 K) in aerated water solutions, and pH was adjusted using $HClO_4$ or NaOH.

2.6. Electromotive force measurements

Potentiometric measurements were performed using a Metrohm mod. 713 potentiometer (resolution of ± 0.1 mV), coupled with a Metrohm 765 Dosimat burette (minimum deliverable volume of ± 0.001 cm^3) and equipped with a Metrohm combined glass electrode (mod. 6.0259.100).

For all the potentiometric measurements the electrode couple was standardized, in terms of pH = $-\log[H^+]$, by titrating a 10 mmol L^{-1} HCl solution (at the same ionic strength value as the solution under study) with standard KOH, in order to determine the formal potential E^0 before each experiment. All the potentiometric titrations were carried out in a stream of purified nitrogen, gently bubbled in the titration cell to avoid O_2 and CO_2 contamination. The measurement cells were thermostated at 25 ± 0.1 °C by means of water circulation from a thermocryostat (mod. D1-G Haake, Victoria, Australia). The titrations were carried out upon addition of TEACl to reach a ionic strength of 0.01 mol L^{-1}. TEACl was used to control the ionic strength, because this salt does not interact significantly with the negatively charged organic molecules and it is commonly used for the titration of polyelectrolytes (Crea et al. 2009). Each titration was repeated for at least three times.

Alkalimetric titrations were performed on: *(i)* solutions containing 1.0 mmol L^{-1} L-tyrosine (tyrOH), to assess the protonation constants of the amino acid in the experimental conditions reported above, and *(ii)* solutions with 1.0 mmol L^{-1} tyrOH and Cu^{2+}, with molar ratios tyrOH/Cu^{2+} of 1 or 2, in order to evaluate the complexation constants of the complexes tyrOH/Cu^{2+}. A second series of alkalimetric titrations were performed on: *(i)* 1.0 mmol L^{-1} tyrOH solutions irradiated for 16, 24 or 72 h, in order to assess the proton exchange capacity of the irradiated material, and *(ii)* 1.0

mmol L^{-1} tyrOH solutions irradiated for 24h, with the addition (after irradiation) of 0.5-1.0 mmol L^{-1} Cu^{2+}, to assess the copper complexation capacity of the by-products derived from the photodegradation of the aminoacid. The solutions were titrated with 0.1 mol L^{-1} KOH standard solution, up to pH 11.5. In some cases, 1.0-1.5 mmol L^{-1} HCl was added before the titration procedure in order to lead the solutions in acidic conditions and allow the protonation of the most acidic functions of the organic molecules. The tyrOH and Cu^{2+} concentrations were chosen so that they were suitable for both the potentiometric measurements and the photochemistry studies.

2.7. Data analysis and calculations

To determine the electrode parameters from calibration data, the calculations were performed by using the non-linear least squares computer program ESAB2M (De Stefano et al., 1987). This program allows the refining of the analytical concentration of the reagents, the electrode formal potential E^0 and the ionic product of water K_w.

The BSTAC software (De Stefano et al., 1993) was used to elaborate the titration data and estimate protonation constants, acidic sites concentrations and complexation constants (more details on the elaboration process and on the expression of the formation constants are reported in the *Supplementary Content* file) . The species distribution diagrams were obtained by using a specific software (ES4ECI; De Stefano et al., 1989).

3. Results

3.1. Phototransformation of L-tyrosine (tyrOH)

The irradiation of 1 mmol L^{-1} tyrOH (pH 5.9) caused its transformation with half-life time of 16 h and 95% degradation in 72 h. No transformation was observed in the dark at the same time scale. The diagram with the phototransformation trend is reported in the *Supplementary Material file*

(Figure S1). The formation of nitrite, nitrate and ammonium during irradiation was also monitored. After 24 h the nitrite concentration was negligible, while the nitrate and ammonium concentrations were $1.2 \cdot 10^{-6}$ and $6.7 \cdot 10^{-6}$ mol L^{-1}, respectively. The turbidity of the solutions obtained after irradiation was determined nephelometrically, and the diameters of possible particles formed were measured by Dynamic Laser Light Scattering. These measures allowed the exclusion of significant particle formation upon tyrOH irradiation.

3.2. Spectroscopic characterization of the irradiated systems

In agreement with previous investigations (Bianco et al., 2014), the tyrOH absorption band at 275 nm decreased in intensity during irradiation (compared to the background that, however, was not constant during these experiments). The spectra reported in Figure 1b actually show a general absorbance increase that was extended into the visible (irradiated solutions appeared pale yellow). The spectra are exclusively accounted for by radiation-absorbing species, because the presence of particles was excluded. Interestingly, the featureless exponential decay of the absorbance above 300 nm at 16-72 h irradiation is quite similar to the typical absorption spectra of HS in the same wavelength region (Galgani et al., 2011).

The EEM spectra of a solution of 1.0 mmol L^{-1} tyrOH, before irradiation and after different irradiation times, are reported in Figure 2. Before irradiation, the EEM spectrum (Figure 2a) shows the typical tyrosine peaks at Excitation/Emission wavelengths (Ex/Em) of 200/300 and 240–290/300–340 nm. Upon irradiation one observes a progressive decrease of the intensity of the tyrosine signal, and the appearance of new peaks at Ex/Em=240-260/390–430 and 270–320/390–480 nm (Figure 2b and 2c).

After 72 hours of irradiation the intensity of almost all the fluorescence signals was considerably decreased compared to e.g. 24 h irradiation, with the exception of the fluorescence emission signals above 475 nm. Fully comparable results were obtained for the irradiation of tyrOH at the own pH (~ 3.9), and at pH 7 adjusted with a phosphate buffer.
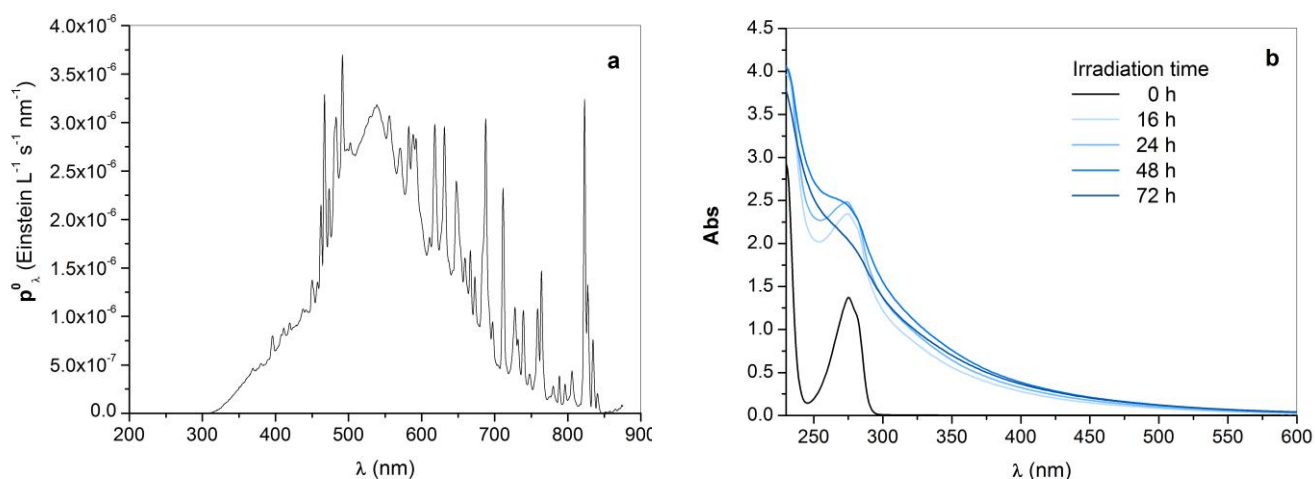
13

Figure 1. a) Lamp photon flux density ($p°_\lambda$) incident on the irradiated solutions. b) Absorption spectra of 1 mmol L^{-1} tyrOH, before irradiation and after different irradiation times.
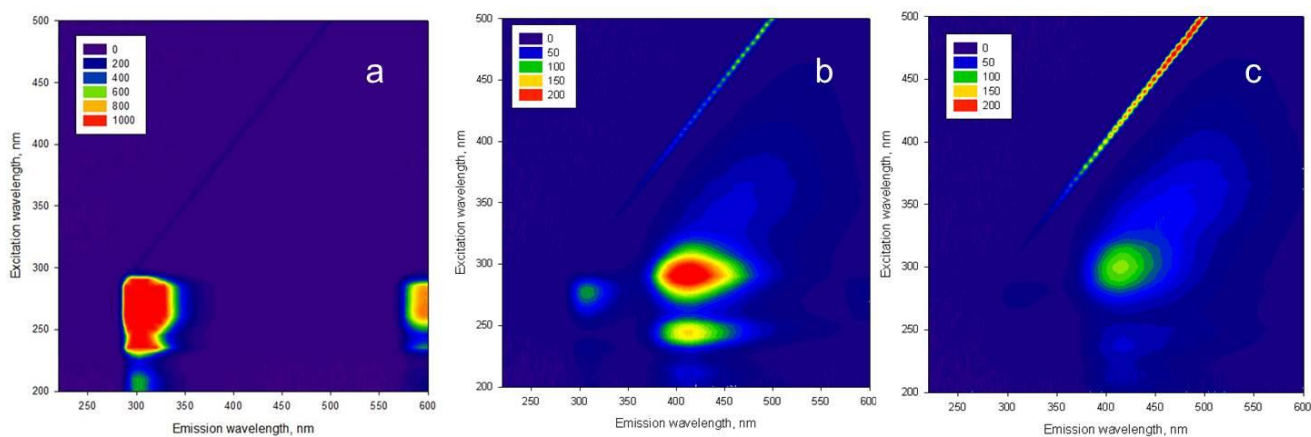

Figure 2. EEMs of tyrOH (initial concentration 1 mmol L^{-1}) at different irradiation times: (a) 0 h, (b) 24 h, (c) 72 h. The linear features are the first and second harmonic of the Rayleigh–Tyndall scattering (emission wavelength equal to or double than the excitation wavelength), and the Raman scattering of water (Baker, 2002).

The NMR spectra reported in Figure 3 show the formation of new signals in the aromatic range at 6.8-7.5 ppm. These three singlets (∂ 7.41, 7.15, 6.90 ppm) could be attributed to aromatic hydrogens shifted by the insertion of functional groups on the aromatic ring. The other signals can be assigned to the unreacted tyrosine or to species where some proton does not differ significantly from the former tyrosine .

3.3. MS characterization

The MS direct infusion analysis of the degradation products of a solution of 1.0 mmol L^{-1} tyrOH after 24 h irradiation showed the signals reported in Table 1. The peaks at *m/z* 182 and 198 would correspond to the [M+H$^+$] ion of tyrOH and to the mono-hydroxylated derivative (tyr(OH)$_2$). The signal at *m/z* 361 is probably due to a dimeric species, such as tyrO-tyrOH. It is possible to propose the structure of the dimer on the basis of the MS^2 and MS^3 data. Table 1 shows the fragments obtained from *m/z* 361: *m/z* 344, 327 and 315. These ions correspond to neutral losses of one or two NH$_3$, or HCOOH, respectively. The fragmentation of the ion *m/z* 315 gives the ions with *m/z* 298, 269 and 254 (see Table 1). These ions correspond again to the neutral losses of NH$_3$, HCOOH and of both CO_2 and NH$_3$. The fragmentations prove the integrity of the amino-acidic groups in the dimeric structure, which suggests that the dimerization would involve the phenolic moiety of tyrOH and not the formation of a peptide bond. Table 1 also reports a structure proposed for the ion with *m/z* 361.
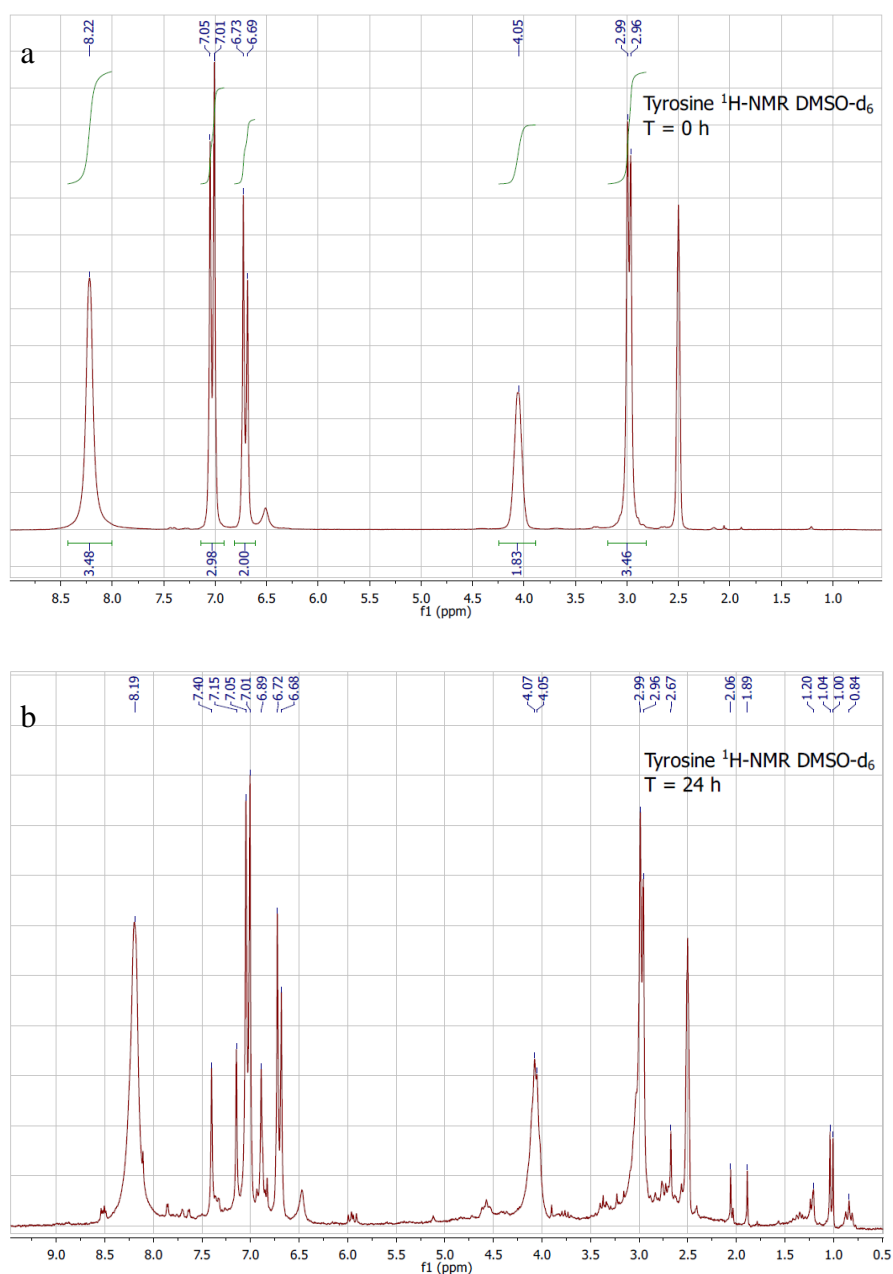
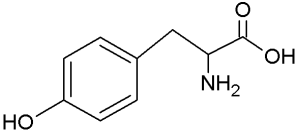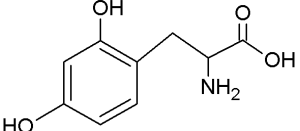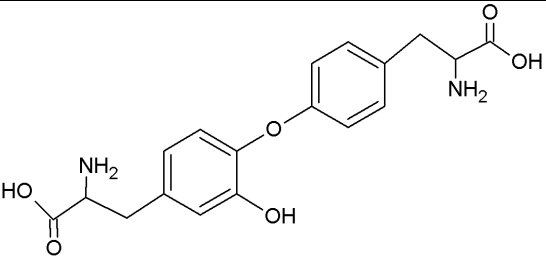**Figure 3.** ^{1}H-NMR spectra of acidified L-tyrosine before (a) and after 24 h of irradiation (b) (DMSO-d^6). ^{1}H NMR (200 MHz, DMSO-d$_6$): δ 8.20 (1H, s, <u>H</u>OPh), 7.03 (2H, d, J 8.1 Hz, CHPh), 6.71 (2H, d, J 8.1 Hz, CHPh), 4.07 (1H, m, CH$_2$-C<u>H</u>), 2.98 (2H, d, J 6.0 Hz C<u>H</u>$_2$-CH).

Table 1. MS direct infusion analysis of the degradation products of a solution of L-tyrosine 1.0 mmol L^{-1} after 24 h.

Acronym	$[M-H]^+$ m/z	Structure	Sum Formula	MS/MS	MS^3
tyrOH	182		$C_9H_{11}NO_3$	165 (-17)	-
tyr(OH)$_2$	198		$C_9H_{12}NO_4$	181 (-17)	-
tyrO-tyrOH	361		$C_{18}H_{20}N_2O_6$	**361** 344 (-17) 327 (-34) 315 (-46)	**315** 298 (-17) 269 (-46) 254 (-61)

3.4. Laser flash photolysis experiments

The 266-nm laser irradiation of 2 mmol L^{-1} tyrOH yielded a rather complex absorption spectrum (see Figure 4), which suggests the occurrence of several transient species. The absorption above 500 nm is probably the combination of multiple contributions by tyrosine triplet state (^{3}tyrOH*), the radical cation tyrOH$^{+\bullet}$ (formed by tyrOH photoionization), and the aquated electron (Bent and Hayon, 1975). All these species appear to undergo decay with similar kinetics, which makes it difficult to distinguish the individual decays. However, the signal at 400 nm is probably due to the phenoxy radical of tyrOH (tyrO$^\bullet$) (Tang et al., 2012). The species tyrO$^\bullet$ could be formed upon photoinduced breaking of the O-H bond in the phenolic group of tyrosine, or by deprotonation of tyrOH$^{+\bullet}$.
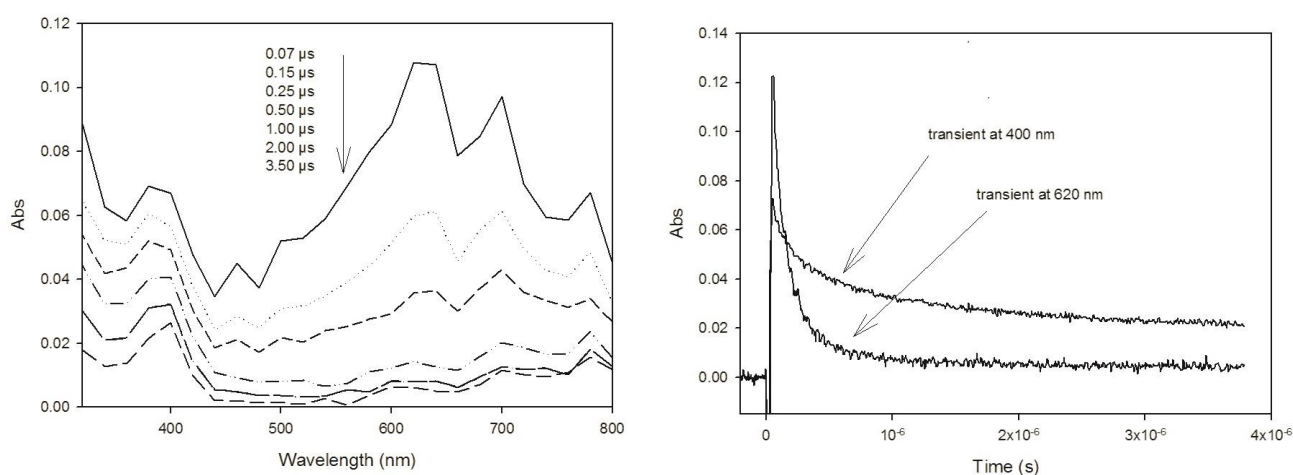

Figure 4. Left: Transient absorption spectra obtained upon 266 nm excitation of a 2 mM tyrOH solution in water at pH 6.5. The various curves represent the laser flash photolysis traces at different times after the laser pulse (indicated in the figure legend). Right: time decay of signals at 400 and 620 nm (same experimental conditions as above).

3.5. Protonation equilibria

The titration curves obtained with tyrOH irradiated for 16, 24 and 72 hours show a quite different trend compared to those obtained with the same compound in the absence of irradiation, as shown in Figure 5. The photodegradation process led to a progressive acidification of the solutions (see the initial pH, corresponding to $V_{KOH} = 0$ mL, at the different irradiation times).

The alkalimetric titration data were elaborated with the BSTAC software. The protonation constants of non-irradiated tyrOH were calculated based on the same experimental conditions as for the irradiated solutions. The results for tyrosine before irradiation (see Table 2) are in good agreement with the literature data (Martell and Smith, 1989). The acidic constants allow the identification of the amino-acidic carboxy group, the amine function and the phenolic hydroxyl.

For the irradiated solutions, a chemical model was proposed and the protonation constants, $\log K^H$, were calculated. A discrete model, where the molecules are supposed to contain a series of discrete sites with different independent $\log K^H$ values, was used to account for the experimental data. In order to fit satisfactorily the titration curves, a model with three protogenic sites (hereafter A, B, C) was proposed. It was possible to explain, with the same model, the experimental data obtained with tyrOH irradiated for 16, 24 or 72 hours, which suggests that certain groups would be formed upon irradiation and would not change very much thereafter. The proposed concentrations and protonation constants of the sites are reported in Table 2. On the basis of the $\log K^H$ values, one can reasonably associate site A to an alkylic or aromatic carboxylic function that has no amino-acidic nature and, quite probably, the sites B and C to an amine function (not necessarily amino-acidic) and to a phenol group, respectively. Isolated carboxy functions can be formed from irradiated tyrosine by deamination, which is consistent with the formation of ammonium. Concerning the phenol functions, there is NMR and MS evidence of the formation of further phenolic groups in addition to those typical of tyrosine.

The uncertainties associated with the $\log K^H$ values and reported in Table 2 are related to the goodness of the fit, but they do not take into account the uncertainty due to the entire experimental procedure. By averaging the $\log K^H$ values obtained upon elaboration of each single titration curve, one gets a more reliable value of 0.3 for the standard deviations of all the protonation constants.

Figure 6 reports the concentration of the protogenic sites calculated as a function of the irradiation time. It is possible to note that there is an increase of the concentrations for each site upon irradiation. The site concentrations ranged between $2.5 \cdot 10^{-4} - 4.5 \cdot 10^{-4}$ mol L^{-1} for A and B, and between $5 \cdot 10^{-4} - 1 \cdot 10^{-3}$ mol L^{-1} for C.

Table 2. Chemical models and protonation constants of acidic sites obtained from the elaboration of titration data of 1.0 mmol L^{-1} tyrOH, and of 1.0 mmol L^{-1} tyrOH irradiated. $I = 0.01$ mol L^{-1} (adjusted by addition of TEACl), $t = 25°C$.

Sample	Acidic site	$\log\beta$ [a]	$\log K$ [a]	$\log K$ [b]
L-tyrosine	tyrOH	10.30 ± 0.01[c]		10.31
	HtyrOH	19.38 ± 0.01	9.08	9.04
	H$_2$tyrOH	21.58 ± 0.02	2.20	2.17
	weighted standard deviation of the fit[d]	1.47		
	total no. of points	253		
Irradiated L-tyrosine	*A*	4.76 ± 0.02		
	B	8.84 ± 0.02		
	C	10.51 ± 0.02		
	weighted standard deviation of the fit	2.28		
	total no. of points	409		

[a] The protonation constants are expressed as log of the cumulative constant $\beta_r = [AH_r^{-n+r}]/[A^{-n}][H^+]^r$ or of the stepwise constant $K = [AH_r^{-n+r}]/[H_{r-1}A^{-n+r-1}][H^+]$. The $\log K$ are calculated from $\log\beta$, for example $\log K(H_2tyrOH) = \log\beta(H_2tyrOH) - \log\beta(HtyrOH)$, and are reported only when different from $\log\beta$.
[b] Ref. Martel and Smith, 1989. Values recalculated at $I = 0.01$ mol L^{-1} by the application a Debye-Hückel expanded function (Casale et al., 1988).
[c] Uncertainty obtained from the software elaboration.
[d] Weight for each experimental point is given as $w = 1/s^2$ (De Stefano et al. 1993).
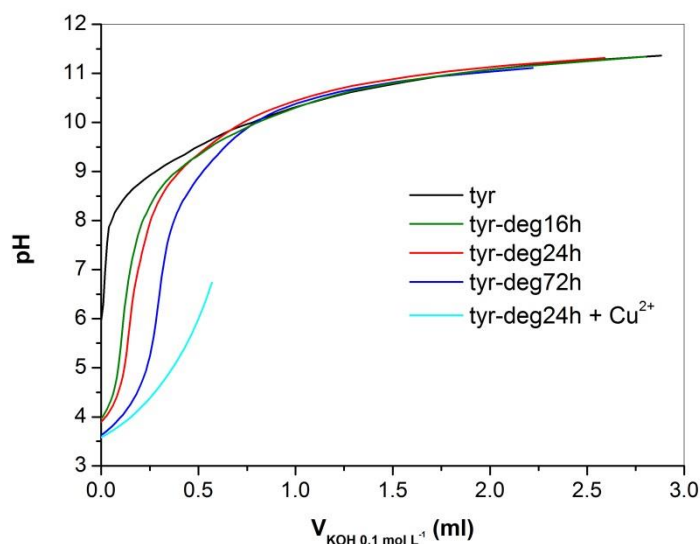
Figure 5. Titration curves of: 1.0 mmol L^{-1} tyrOH, not irradiated (black curve); 1.0 mmol L^{-1} tyrOH, irradiated for 16 h (green curve); 1.0 mmol L^{-1} tyrOH, irradiated for 24 h (red curve); 1.0 mmol L^{-1} tyrOH, irradiated for 72 h (blue curve); 1.0 mmol L^{-1} tyrOH, irradiated for 24 h and added with 0.5 mmol L^{-1} $CuCl_2$ (light cyan curve). Titrant: KOH 0.1 mol L^{-1}; ionic strength 0.01 mol L^{-1} (TEACl); temperature 25°C.

Figure 6. The concentration of the protogenic sites, as a function of the irradiation time, calculated upon application of the chemical model reported in Table 2.
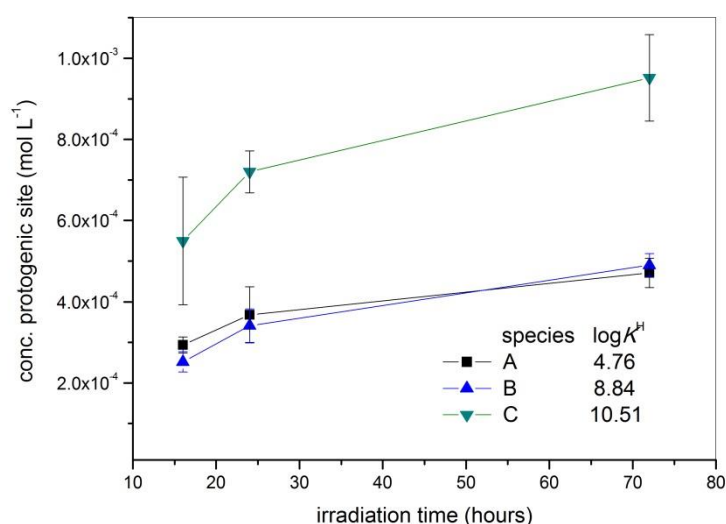
3.6. Copper complexation.

Solutions of 1.0 mmol L^{-1} tyrOH (non irradiated), and of 1.0 mmol L^{-1} tyrOH irradiated for 24 h, were titrated with KOH 0.1 mol L^{-1} upon addition of $CuCl_2$. In both cases a marked acidification was observed compared to the curves obtained without Cu^{2+} addition (see Figure 5, comparing the same irradiation time). Acidification is reasonably due to proton release associated to the complexation of Cu^{2+} by tyrOH or/and by its photodegradation products. Precipitation of copper hydroxide took place at pH ~ 6, thus the experiments were carried out only until pH 6 and, prudentially, only the data up to pH 5.5 were elaborated.

The alkalimetric titration data were elaborated with the BSTAC software, and a chemical model was proposed to calculate the stability constants of the complexes, $\log\beta$. The relevant data are reported in Table 3. The results obtained with non-irradiated tyrOH are in quite good agreement with the literature data, and the complexes formed have the stoichiometry Cu-tyrOH and Cu(tyrOH)$_2$, where tyrOH is the L-tyrosine that still has the phenolic proton (Pettit, 1984).

The trend of the titration curves obtained with the irradiated solutions can be explained by hypothesizing the formation of two complexes with stoichiometry Cu*A* and Cu*B*, where *A* and *B* are the protogenic sites reported in Table 2. Calculations were obviously performed by considering the formation of hydrolytic species of the copper cation. Among the latter they were taken into account $[Cu(OH)]^{+}$, $[(Cu)_2(OH)_2]^{2+}$, $[Cu(OH)_3]^{-}$, $[Cu(OH)_4]^{2-}$, with respective formation constants $\log\beta^{Cu(OH)}$ = -7.70, $\log\beta^{Cu2(OH)2}$ = -10.75, $\log\beta^{Cu(OH)3}$ = -27.12, and $\log\beta^{Cu(OH)4}$ = -39.83 (I = 0.1 mol L^{-1}, t = 25°C) (Smith et al., 2001). To elaborate the data obtained on the irradiated solutions, the residual tyrOH was also considered. It was quantified by HPLC on each solution, and the relevant tyrOH concentration was used as fixed input datum in the elaboration process, together with the protonation constants measured before. In the experimental pH range, the complexation involving the phenolic group (Cu*C*) could be excluded.

Upon consideration of the values of the complex formation constants, the insertion of at least a second donor group in the metal coordination looks quite likely. The value of the stability constant of Cu*A*

suggests the contribution of a second carboxylate group or of an aromatic amine (SC-Database, v. 5.84). In this case, on the basis of previous information, it is more probable the insertion of a second carboxylate. The formation constant of Cu*B* has a value that is similar to those of Cu-amino-acid complexes, where the copper cation is coordinated by both amino and carboxylate functions (SC-Database, v. 5.84). In both cases, the lack of evidence of a second proton release within the coordination process suggests that the second carboxylic function is inserted in an amino-acidic structure having a low protonation constant.

On the basis of the formation constants reported in Table 3, it is possible to calculate the percentage of metal involved in the complexes (see Figure S2 in the *Supplementary Material file*) and to note that the degraded mixture has a higher binding capacity than the parent amino-acid.

The experimental Cu concentration (0.5-1 mM) was chosen to enable the measurement of complexation constants by means of potentiometric titration. In these conditions, the precipitation of $Cu(OH)_2$ around pH 6 in the experimental system is unavoidable, but under natural water conditions one has lower Cu levels. Therefore, in the natural environment there would be higher probability that Cu occurs in the dissolved phase where complexation by naturally-occurring ligands could play a major role. We thus tried to assess the possible effect of dissolved organic material arising from tyrOH photodegradation, on the copper distribution in natural waters. To do so, simulations were done on the basis of the stability constants of copper complexes with the degraded amino acid (determined in this work) and with the main components of water, such as hydroxide, chloride, carbonate and phosphate anions (see Figure 7; the stability constants used for the simulation are reported in Table S1 of the *Supplementary Material file*). We simulated the copper speciation, between pH 5 and 9, for a water containing chloride $1 \cdot 10^{-4}$ mol L^{-1}, carbonate $1 \cdot 10^{-5}$ mol L^{-1}, and phosphate $1 \cdot 10^{-5}$ mol L^{-1}, as a function of the total ligand (L) concentration. Here L has the same properties as the DOM derived from the photodegradation of tyrOH, and its concentration was assumed to range between $1 \cdot 10^{-6}$ and $1 \cdot 10^{-1}$ mol L^{-1}. In terms of ligand groups, L was assumed to be composed of 0.25 *A*, 0.25 *B* and 0.5 *C*. This assumption allowed us to maintain the same concentration ratios between the components *A*, *B* and *C*, as those obtained from the titration elaboration. Two concentration levels of copper were taken

into consideration, namely $1 \cdot 10^{-6}$ and $1 \cdot 10^{-8}$ mol L^{-1}. The upper limit may be representative of polluted natural waters (Zeng et al., 2015) and, additionally, it gives insight into the ability of the photogenerated organic ligands to prevent the precipitation of Cu(OH)$_2$. The presence of cations that could compete with copper coordination was not taken into consideration. To simulate the natural environment, the pH and Cu concentration range used in the simulations were quite far from the experimental conditions by which the speciation model was obtained. Therefore, it is not possible to exclude the presence of other complex species not detected in the experiments. Examples of such species are CuL$_n$ (the occurrence of which is more likely with an excess of the ligand), or complexes where the phenolic or hydroxide groups participate to the metal coordination (which is likely for pH > 7). Despite this strong simplification, from the diagrams proposed in Figure 7 it is possible to note that the CuB complex would be the predominant species in a wide range of pH values and of Cu and ligand concentrations. The aqua ion (Cu$^{2+}_{aq}$) becomes important at low log[L] and low pH, whereas at high pH the hydrolytic species gain importance with the precipitation of copper hydroxide or with the formation of the complex [Cu(OH)]$^+$ (see Figure S3 in the *Supplementary Material file*). Moreover, the ligands can totally avoid the hydroxide precipitation when the Cu concentration is $1 \cdot 10^{-8}$ mol L^{-1}.

Table 3. Chemical models and stability constants of the complexes of Cu^{2+} with L-tyrosine, and with L-tyrosine irradiated for 24 h. $I = 0.01$ mol L^{-1} (TEACl), $t = 25$°C.

Sample	Species	logβ [a]	log$K$ [b]	log$K$ [c]
L-tyrosine	CutyrOH	18.42 ± 0.02	8.12	8.0
	Cu(tyrOH)$_2$	36.12 ± 0.03	15.54	14.8
	weighted standard deviation of the fit[d]	2.14		
	total no. of points	92		
L-tyrosine degraded	CuA	3.80 ± 0.03		
	CuB	8.38 ± 0.03		
	weighted standard deviation of the fit	0.73		
	total no. of points	174		

[a] Refer to the general reaction: pCu$^{2+} + q$L$^{z-} + r$H$^+ \leftrightarrows$ [Cu$_p$L$_q$H$_r$] $^{2p+r-qz}$.

[b] log$K$ values were calculated from logβ values and refer to the reaction: pCu$^{2+}+q$H$_r$L$^{r-z} \leftrightarrows$ [(Cu)$_p$(H$_r$L)$_q$]$^{2p+q(r-z)}$, where a reagent is the protonated ligand and z is the charge of the fully deprotonated ligand.

[c] Ref. (Pettit, 1984). Values recalculated at $I =0.01$ mol L^{-1} by the application a Debye-Hückel expanded function (Casale et al., 1988).

[d] Weight for each experimental point is given as w = $1/s^2$ (De Stefano et al., 1993).
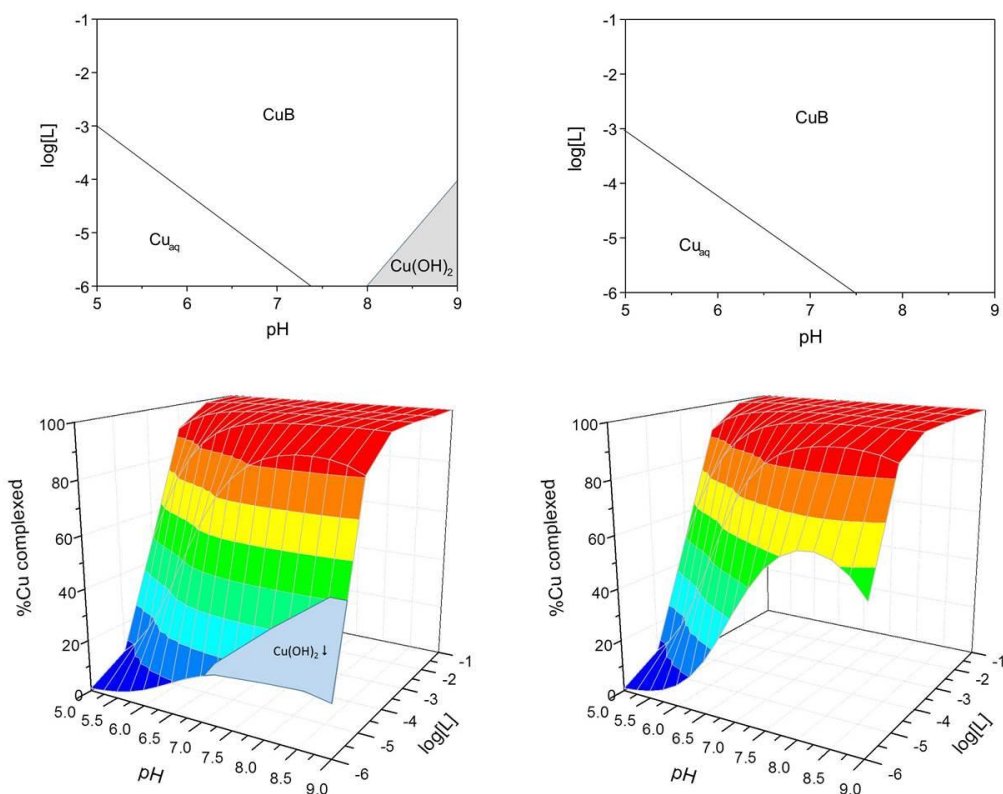
Figure 7. Distribution diagrams of copper in a simulated natural water, as a function of the concentration of the ligand (L), derived from the photodegradation process, and of pH. Total Cu(II) concentration: $1 \cdot 10^{-6}$ (left) and $1 \cdot 10^{-8}$ mol L^{-1} (right). The diagrams at the top of the figure report the predominant species for different values of log[L] and pH.

4. Discussion

Most of the knowledge about the structure of HS has been provided by the NMR e FT-IR spectroscopies (Albers, 2010; Fooken, 2003), given their capacity to identify functional groups. Conversely, fluorescence spectroscopy is a useful technique for routine analysis aimed at the identification of these macromolecules in environmental samples (Coble, 1996; Barsotti et al., 2016). However, none of these techniques is able to supply a complete description of the nature of HS. Therefore, in order to obtain a reliable description of the size, structure and chemistry of HS, or HULIS, more than one technique is necessary. The results reported before, obtained from the application of different independent techniques, are consistent with one another and prove that the

tyrosine photo-transformation process yields substances with spectroscopic and chemical behavior similar to those of HS.

Based on the literature, the fluorescence signals obtained with the irradiated solutions fall in the range of HS (Coble, 1996). Given their fluorescence properties, the relevant species should have higher molecular weight compared to the starting substrate (Gao et al., 2011). These remarks are not sufficient to prove the humic–like nature of the photo-transformation products, therefore the system was studied by the application of other techniques. The results obtained by laser flash photolysis and MS can be related with the fluorescence data. The phenoxy-type radical, tyrO$^\bullet$ has the tendency to dimerize (Chiron et al., 2009), and it could account for the detection of dimeric species (tyrO-tyrOH) in MS experiments. Moreover, radicals derived from dimeric species, if formed, could then produce tyrosine oligomers (Net et al., 2009). These phenolic oligomers (with $\geq$ 3 aromatic rings) are potential candidates as HS fluorophores because they are expected to emit fluorescence radiation near 450 nm, independent of the actual number of rings (Barsotti et al., 2016). Oligomeric species of tyrOH, which could be reasonably produced but that were unfortunately not detected in MS experiments, might thus possibly account for the fluorescence emission at 400-450 nm by the irradiated material (see Figure 2). The investigation reveals that the preferential pathway followed by tyrosine during the photo-transformation process is the hydroxylation of the aromatic ring. This finding is proved by NMR, MS and potentiometry. The same data reveal also that the amino acidic functions are not so much affected by the photo-induced reactions. The main species, detected by MS, show unbroken amino acidic functions and the NMR signals (∂ 4.07 and 2.98 ppm) can be assigned to the unreacted tyrosine or to species where some proton does not differ significantly from the tyrosine, such as the dimer tyrO-tyrOH (Table 1) or oligomeric species. This assignation has been attempted by ab-initio calculation (Gaussian 03W, optimization B3LYP 6-31+G(d,p), NMR GIAO/B3LYP 6-311+G(d,p)). Also the potentiometric study reveals the presence of phenolic, carboxylic and amino groups in the irradiated material, which suggests a close similarity with the functional groups of HS (Croue et al., 2003; Klucakova and Kalina, 2015). Of course the same functionalities do also occur in non-irradiated tyrOH, but the formation of non-amino-acidic carboxyls (site *A*) and the rise of phenolic functions

under irradiation increases the humic-like nature of the photogenerated material (Klucakova and Kalina, 2015). Moreover, the Cu*B* would be the major complex form with *B* as an amino ligand. This finding suggests a further analogy between the photogenerated humic-like substances and HS, where the Cu complexation would mainly involve a nitrogenous (and most likely an amino) group (Croue et al., 2003).

5. Conclusions

The phototransformation of L-tyrosine proceeds via deamination with release of free ammonium, hydroxylation of the aromatic ring and dimerisation, the latter presumably triggered by the photochemical formation of tyrosyl radicals that have the tendency to dimerise. The photoprocessed material can form complexes with Cu, to a considerably higher extent compared to the original L-tyrosine. Cu complexation would presumably involve the amino groups of the photoprocessed material, which represent another similarity with humic substances (HS) that carry out copper binding by means of nitrogenous functional groups.

The characterization of the material produced upon direct photolysis of L-tyrosine, which was carried out in the present work with a wider range of techniques than ever before, suggests that the distinction between the photogenerated humic-like material and HS would be very difficult to say the least. Therefore, considering that the definition of HS is mainly operational and based on characterization procedures, which would hardly distinguish between the photogenerated humic-like material and HS, we suggest that an abiotic (photochemical) pathway to HS has been identified in the direct photolysis of amino acids such as L-tyrosine. Such a photohumification pathway has been hypothesised before to account for field data (Brisco and Ziegler, 2004; Ortega-Retuerta et al., 2010), based on the finding that photooxidised aquagenic organic matter can produce humic-like compounds (Kieber et al., 1997), and recent evidence also shows that low-molecular weight dissolved organic nitrogen can be phototransformed into high-molecular weight one (Mesfioui et al., 2015). The present findings, by providing insight into the photohumification process, have important implications for the

photoreactivity and bioavailability of natural organic matter (Santos et al., 2014). L-tryptophan is another aromatic amino acid undergoing photodegradation under UVB (Bianco et al., 2014), and work is currently under way to assess the extent of photohumification induced by tryptophan.

References

Aguer, J. P., Richard, C., 1994. Photochemical behavior of a humic acid synthesized from phenol. J. Photochem. photobiol. A: Chem. 84, 69-73.

Albers, C. N., Hansen, P. E., 2010. ^{13}C-NMR chemical shift databases as a quick tool to evaluate structural models of humic substances. Open Magn. Res. J. 3, 96-105.

Albinet, A., Minero, C., Vione, D., 2010. Phototransformation processes of 2,4-dinitrophenol, relevant to atmospheric water droplets. Chemosphere 80, 753-758.

Amado, A. M., Cotner, J. B., Cory, R. M., Edhlund, B. L., McNeill, K., 2015. Disentangling the interactions between photochemical and bacterial degradation of dissolved organic matter: Amino acids play a central role. Environ. Sci. Technol. 69, 554-566.

Baker, A., 2002. Fluorescence Excitation-Emission Matrix Characterization of river waters impacted by a tissue mill effluent. Environ. Sci. Technol. 36, 1377–1382.

Barsotti, F., Ghigo, G., Vione, D., 2016. Computational assessment of the fluorescence emission of phenol oligomers: A possible insight into the fluorescence properties of humic-like substances (HULIS). J. Photochem. Photobiol. A: Chem. 315, 87-93.

Bent, D. V., Hayon, E., 1975. Excited state chemistry of aromatic amino acids and related peptides. I. Tyrosine. J. Am. Chem. Soc. 97, 2599-2606.

Bianco, A., Minella, M., De Laurentiis, E., Maurino, V., Minero, C., Vione, D., 2014. Photochemical generation of photoactive compounds with fulvic-like and humic-like fluorescence in aqueous solution. Chemosphere 111, 529-536.

Bodrato, M., Vione, D., 2014. APEX (Aqueous Photochemistry of Environmentally occurring Xenobiotics): A free software tool to predict the kinetics of photochemical processes in surface waters. Environ. Sci. Processes Impacts 16, 732-740.

Boreen, A., Edhlund, B., Cotner, J., McNeill, K., 2008. Indirect photodegradation of dissolved free amino acids: the contribution of singlet oxygen and the differential reactivity of DOM from various sources, Environmental Science and Technology 42, 5492–5498.Brisco, S., Ziegler, S.,

2004. Effects of solar radiation on the utilization of dissolved organic matter (DOM) from two headwater streams. Aquat. Microb. Ecol. 37, 197-208.

Bronk, D. A., 2002. Dynamics of DON. Biogeochem. Mar. Dissolved Org. Matter, 153–247.

Casale, A., Daniele, P. G., De Robertis, A., Sammartano, S., 1988. Ionic Strength Dependence of Formation Constants. Part XI. An Analysis of Literature Data on Carboxylate Ligand Complexes. Ann. Chim. (Rome) 78, 249-260.

Cavani, L., Halladja, S., Ter Halle, A., Guyot, G., Corrado, G., Ciavatta, C., Boulkamh, A., Richard, C., 2009. Relationship between photosensitizing and emission properties of peat humic acid fractions obtained by tangential ultrafiltration. Environ. Sci. Technol. 43, 4348-4354.

Cawley, K. M., Korak, J. A., Rosario-Ortiz, F. L., 2015. Quantum yields for the formation of reactive intermediates from dissolved organic matter samples from the Suwannee River. Environ. Eng. Sci. 32, 31-37.

Chiron, S., Barbati, S., Khanra, S., Dutta, B. K., Minella, M., Minero, C., Maurino, V., Pelizzetti, E., Vione, D., 2009. Bicarbonate-enhanced transformation of phenol upon irradiation of hematite, nitrate, and nitrite. Photochem. Photobiol. Sci. 8, 91-100.

Coble, P. G., 1996. Characterization of marine and terrestrial DOM in seawater using excitation–emission spectroscopy. Mar. Chem. 51, 325–346.

Crea, F., De Stefano, C., Gianguzza, A., Pettignano, A., Piazzese, D., Sammartano, S., 2009. Acid-base properties of synthetic and natural polyelectrolytes: Experimental results and models for the dependence on different aqueous media. J. Chem. Eng. Data 54, 589–605.

Croue, J. P., Benedetti, M. F., Violleau, D., Leenheer, J. A., 2003. Characterization and copper binding of humic and nonhumic organic matter isolated from the South Platte River: Evidence for the presence of nitrogenous binding site. Environ. Sci. Technol. 37, 328-336.

De Laurentiis, E., Maurino, V., Minero, C., Vione, D., Mailhot, G., Brigante, M., 2013a. Could triplet-sensitised transformation of phenolic compounds represent a source of fulvic-like substances in natural waters? Chemosphere 90, 881-884.

De Laurentiis, E., Sur, B., Pazzi, M., Maurino, V., Minero, C., Mailhot, G., Brigante, M., Vione, D., 2013b. Phenol transformation and dimerisation, photosensitised by the triplet state of 1-nitronaphthalene: A possible pathway to humic-like substances (HULIS) in atmospheric waters. Atmos. Environ. 70, 318-327.

De Laurentiis, E., Socorro, J., Vione, D., Quivet, E., Brigante, M., Mailhot, G., Wortham, H., Gligorovski, S., 2013c. Phototransformation of 4-phenoxyphenol sensitised by 4-carboxybenzophenone: Evidence of new photochemical pathways in the bulk aqueous phase and on the surface of aerosol deliquescent particles. Atmos. Environ. 81, 569-578.

De Stefano, C., Princi, P., Rigano, C., Sammartano, S., 1987. Computer analysis of equilibrium data in solution. ESAB2M: an improved version of the ESAB program. Ann. Chim. (Rome) 77, 643–675.

De Stefano C., Princi, P., Rigano, C. and Sammartano, S., 1989. The calculation of equilibrium concentrations. ES4EC1. A FORTRAN program for computing distribution diagram and titration curves. Comput. Chem. 13, 343-359.

De Stefano, C., Mineo, P., Rigano, C., Sammartano, S., 1993. Ionic strength dependence of formation constants. XVII. The calculation of equilibrium concentrations and formation constants. Ann. Chim. (Rome) 83, 243–277.

Fooken, U., Liebezeit, G., 2003. An IR study of humic acids isolated from sediments and soils. Senck marit. 32, 183-189.

Galgani, L., Tognazzi, A., Rossi, C., Ricci, M., Angel Galvez, J., Dattilo, A. M., Cozar, A. Bracchini, L., Loiselle, S. A., 2011. Assessing the optical changes in dissolved organic matter in humic lakes by spectral slope distributions. J. Photochem. Photobiol. B: Biol. 102, 132-139.

Gao, L., Fan, D. D., Sun, C. X., Li, D. J., Cai, J. G., 2011. Optical characterization of CDOM in a marsh-influenced environment in the Changjiang (Yangtze River) Estuary. Environ. Earth Sci. 64, 643-658.

He, X. S., Xi, B. D., Pan, H. W., Li, X., Li, D., Cui, D. Y., Tang, W. B., Yuan, Y., 2014. Characterizing the heavy metal-complexing potential of fluorescent water-extractable organic

matter from composted municipal solid wastes using fluorescence excitation-emission matrix spectra coupled with parallel factor analysis. Environ. Sci. Pollut. Res. 21, 7973-7984.

Kieber, D. J., Hydro, L. H., Seaton, P. J., 1997. Photooxidation of triglycerides and fatty acids in seawater: implication toward the formation of marine humic substances. Limnol. Oceanogr. 42, 1454-1462

Klucakova, M., Kalina, M., 2015. Composition, particle size, charge, and colloidal stability of pH-fractionated humic acids. J. Soils Sediments 15, 1900-1908.

Kuhn, H. J., Braslavsky, S. E., Schmidt, R. 2004. Chemical actinometry. Pure Appl. Chem. 76, 2105-2146.

Latch, D. E., McNeill, K., 2006. Microheterogeneity of singlet oxygen distributions in irradiated humic acid solutions. Science 311, 1743-1747.

Ma, J. H., Del Vecchio, R., Golanoski, K. S., Boyle, E. S., Blough, N. V., 2010. Optical properties of humic substances and CDOM: Effects of borohydride reduction. Environ. Sci. Technol. 44, 5395-5402.

Martell, A. E., Smith, R. M., 1989. Critical Stability Constants, Vol. 1, Plenum Press, New York.

Mesfioui, R., Abdulla, H. A. N., Hatcher, P. G., 2015. Photochemical alterations of natural and anthropogenic dissolved organic nitrogen in the York river. Environ. Sci. Technol. 49, 159-167.

Minella, M., Merlo, M. P., Maurino, V., Minero, C., Vione, D., 2013. Transformation of 2,4,6-trimethylphenol and furfuryl alcohol, photosensitised by Aldrich humic acids subject to different filtration procedures. Chemosphere 90, 306-311.

Nebbioso, A., Piccolo, A., 2011. Basis of a humeomics science: Chemical fractionation and molecular characterization of humic biosuprastructures. Biomacromolecules 12, 1187-1199.

Nebbioso, A., Piccolo, A., Lamshoeft, M., Spiteller, M.., 2014. Molecular characterization of an end-residue of humeomics applied to a soil humic acid. RSC Adv. 4, 23658-23665.

Net, S., Nieto-Gligorovski, L., Gligorovski, S., Temime-Rousell, B., Barbati, S., Lazarou, Y. G., Wortham, H., 2009. Heterogeneous light-induced ozone processing on the organic coatings in the atmosphere. Atmos. Environ. 43, 1683-1692.

Ortega-Retuerta, E., Reche, I., Pulido-Villena, E., Agustí, S., Duarte, C. M., 2010. Distribution and photoreactivity of chromophoric dissolved organic matter in the Antarctic Peninsula (Southern Ocean). Mar. Chem. 118, 129-139.

Pettit, L. D., 1984. Critical survey of formation constants of complexes of histidine, phenylalanine, tyrosine, L-DOPA and tryptophan. Pure & Appl.Chem. 56, 247-292.

Piccini, C., Conde, D., Pernthaler, J., Sommaruga, R., 2009. Alteration of chromophoric dissolved organic matter by solar UV radiation causes rapid changes in bacterial community composition. Photochem. Photobiol. Sci. 8, 1321-1328.

Piccolo, A., 2001. The supramolecular structure of humic substances. Soil Sci. 166, 810-832.

Plowman, J. E., Deb-Choudhury, S., Grosvenora, A. J., Dyera, J. M., 2013. Protein oxidation: identification and utilisation of molecular markers to differentiate singlet oxygen and hydroxyl radical-mediated oxidative pathways, Photochemical and Photobiological Science 12, 1960–1967.

Posadaz, A., Biasutti, A., Casale, C., Sanz, J., Arnat-Guerri, F., Garcia, N. A., 2004. Rose bengal-sensitized photooxidation of the dipeptides L-tryptophyl-Lphenylalanine, L-tryptophyl-L-tyrosine and L-tryptophyl-L-tryptophan: kinetics, mechanism and photoproducts, Photochemistry and Photobiology 80, 132-1 38.

Prado, B., Duwig, C., Hidalgo, C., Mueller, K., Mora, L., Raymundo, E., Etchevers, J. D., 2014. Transport, sorption and degradation of atrazine in two clay soils from Mexico: Andosol and Vertisol. Geoderma 232, 628-639.

Santos, L., Santos, E. B. H., Dias, J. M., Cunha, A., Almeida, A., 2014. Photochemical and microbial alterations of DOM spectroscopic properties in the estuarine system Ria de Aveiro. Photochem. Photobiol. Sci. 13, 1146-1159.

Saprygina,N. N., Morozova, O. B., Grampp, G., Yurkovskaya, A. V., 2014. Effect of amino group charge on the photooxidation kinetics of aromatic amino acids, The Journal of Physical Chemistry A 118, 339−349.

SC-Database. The IUPAC stability constant database, version 5.84, Academic Software, Sourby Old Farm, Timble, Otley, Yorks, LS21 2PW, UK.

Senesi, N., 1992. Binding mechanisms of pesticides to soil humic saubstances. Sci Total Environ. 123, 63-76.

Smith, R. M., Martell, A. E., Motekaitis, R. J., 2001. NIST Critical Selected Stability Constant of Metal Complexes Database 46 Version 6.0.

Sommaruga, R., Augustin, G., 2006. Seasonality in UV transparency of an alpine lake is associated to changes in phytoplankton biomass. Aquat. Sci. 68, 129-141.

Su, Y. L., Chen, F. Z., Liu, Z. W., 2015. Comparison of optical properties of chromophoric dissolved organic matter (CDOM) in alpine lakes above or below the tree line: insights into sources of CDOM. Photochem. Photobiol. Sci. 14, 1047-1062.

Tang, R. Z., Li, H. X., Liu, Y. C., Zhang, P., Cao X. Y., Wang, W. F., 2012. Laser flash photolysis study on electron transfer oxidation reaction of tryptophan or tyrosine with triplet state vitamin K-3. Acta Phys. Chem. Sinica 28, 213-216.

Thurman, E. M., 1985. Organic Geochemistry of Natural Waters, chapter 6, pp. 151-155.

Turro, N. J., Ramamurthy, V., Cherry, W., Farneth, W., 1978. The effect of wavelength on organic photoreactions in solution. Reactions from upper excited states, Chem. Rev. 78, 125-145.

Uusikivi, J., Vahatalo, A. V., Granskog, M. A., Sommaruga, R., 2010. Contribution of mycosporine-like amino acids and colored dissolved and particulate matter to sea ice optical properties and ultraviolet attenuation. Limnol. Oceanogr. 55, 703-713.

Westerhoff, P., Nowack, B., 2013. Searching for global descriptors of engineered nanomaterial fate and transport in the environment. Acc. Chem. Res. 46, 844-853.

Xiao, Y. H., Sara-Aho, T., Hartikainen, H., Vahatalo, A. V., 2013. Contribution of ferric iron to light absorption by chromophoric dissolved organic matter. Limnol. Oceanogr. 58, 653-662.

Xu, S., Zheng, G. D., 2003. Variations in radiocarbon ages of various organic fractions in core sediments from Erhai Lake, SW China. Geochem. J. 37, 135-144.

Zeng, X. X., Liu, Y., You, S. H., Zeng, G. M., Tan, X. F., Hu, X. J., Hu, X., Huang, L., Li, F., 2015. Spatial distribution, health risk assessment and statistical source identification of the trace elements in surface water from the Xiangjiang River, China. Environ. Sci. Pollut. Res. 22, 9400-9412.